ORIGINAL ARTICLE



Light and nutrient cues elicit metabolic reprogramming by targeting carbon fixation, redox balance, and ATP homeostasis in *Agastache rugosa*

Khairul Azree Rosli¹ · Azizah Misran¹ · Latifah Saiful Yazan² · Puteri Edaroyati Megat Wahab¹

Received: 9 January 2025 / Accepted: 29 April 2025 / Published online: 10 May 2025 © The Author(s), under exclusive licence to Springer-Verlag GmbH Germany, part of Springer Nature 2025

Abstract

Main conclusion The study uncovers how *Agastache rugosa* coordinates carbon fixation, redox balance, and ATP homeostasis via distinct metabolic strategies optimized for different light and nutrient conditions.

Abstract This study explores the metabolic adaptations of *Agastache rugosa* (Fisch. & C.A.Mey.) Kuntze in varying light and nutrient conditions, focusing on the coordination between photosynthetic and respiratory pathways. Plants were grown under two light levels (high light, 0% shade; low-light, 50% shade) and four nutrient treatments (NPK1, 40 mg kg⁻¹; NPK2, 80 mg kg⁻¹; NPK3, 120 mg kg⁻¹; NPK4, 160 mg kg⁻¹) and key metabolic parameters were analyzed. High-light plants had peak carbonic anhydrase activity (5.17±0.26 U g⁻¹ FW) at NPK2, optimizing carbon fixation and redox balance with 20.6% and 12.8% higher NADP+/NADPH and NAD+/NADH ratios, each. Low-light plants upregulated PEPC (+110%), and PEPCK (+34%) at NPK4, displaying enhanced anaplerotic carbon fixation. Despite lower respiratory activity, (NADH–UQ, –50%; COX, –46%), plants under low-light had tenfold higher ATP at NPK3 through reduced consumption. Principal component and hierarchical cluster analyses (>60% similarity) revealed distinct metabolic strategies between light treatments. Strong correlations among photosynthetic, respiratory, and redox parameters (r>0.7, P<0.001) indicated metabolic integration via shared regulatory networks. Our findings reveal the metabolic plasticity of *A. rugosa*, offering insights into plant adaptation with implications for cultivation. Moreover, multivariate analyses unveiled complex regulatory networks coordinating energy metabolism, highlighting the metabolic reprogramming employed by *A. rugosa* to maintain energetic and redox balance under dynamic environmental conditions.

 $\textbf{Keywords} \ \ An aplerotic \ pathways \cdot Electron \ transport \ chain \cdot Mitochondrial \ respiration \cdot NADPH/NADP^+ \ ratio \cdot Plant \ adaptation$

Abbreviations

CA Carbonic anhydrase
COX Cytochrome c oxidase

HL High light

Communicated by Dorothea Bartels.

- Khairul Azree Rosli gs47405@student.upm.edu.my; khairulazreerosli@gmail.com
- Department of Crop Science, Faculty of Agriculture, Universiti Putra Malaysia (UPM), 43400 Serdang, Selangor, Malaysia
- Department of Biomedical Sciences, Faculty of Medicine and Health Sciences, Universiti Putra Malaysia (UPM), 43400 Serdang, Selangor, Malaysia

LL Low light

NADH-UQ NADH-ubiquinone oxidoreductase
PCA Principal component analysis
PDC Pyruvate dehydrogenase complex
PEPC Phosphoenolpyruvate carboxylase
PEPCK Phosphoenolpyruvate carboxykinase

Introduction

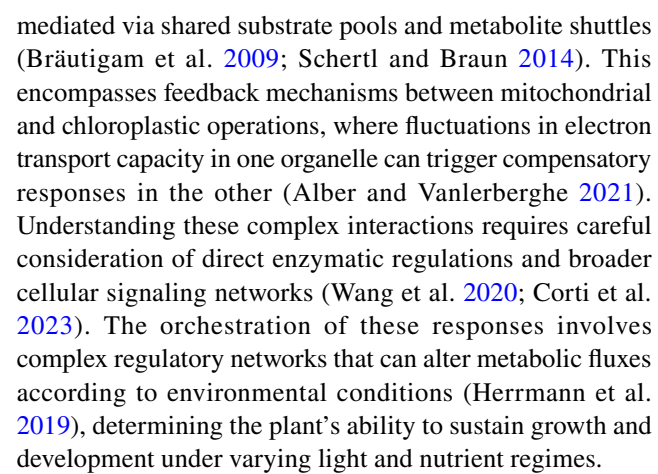
Plants continuously adapt their metabolism to optimize their growth and survival under different environmental conditions (Weng et al. 2021; Zandalinas et al. 2022). The interaction between light and nutrient availability represents one of the most fundamental challenges in plant adaptation, requiring distinct metabolic reprogramming to maintain cellular



homeostasis and energy balance (Scheibe 2019; Artins and Caldana 2022). This metabolic plasticity involves coordinated changes across multiple pathways, including photosynthetic carbon fixation, respiratory metabolism, and cellular redox systems (Suzuki et al. 2012; Shen et al. 2016). Recent advances in understanding plant metabolic networks have shown that these adaptations extend far beyond simple adjustments in individual pathways, encompassing complex regulatory networks that integrate environmental signals with cellular metabolism (Cardoso et al. 2023; Li et al. 2024). The cellular response to changing light conditions, in particular, requires precise coordination between photosynthetic and respiratory pathway components, involving feedback mechanisms that modulate electron transport chains, alter carbon fixation capacity, and maintain optimal energy status via both transcriptional and post-translational regulation (He et al. 2023; Gollan et al. 2023). However, our understanding of how these integrative networks operate in non-model plant species remains limited.

The relationship between light and nutrient use is a critical nexus in plant metabolism, especially involving carbon and nitrogen metabolism (Nunes-Nesi et al. 2010; Sathee et al. 2024). Under different light conditions, plants must balance their investment in photosynthetic machinery with the maintenance of other essential metabolic processes (Jänkänpää et al. 2012; Dahal et al. 2016). This balance is crucial when considering the allocation of nutrients, particularly nitrogen, which is required for both, photosynthetic proteins and other metabolic enzymes (Shi et al. 2015; Ghimire et al. 2017). The modulation of carbon fixation pathways in response to light availability involves the coordination of key photosynthetic enzymes and supporting metabolic networks, including anaplerotic carbon fixation and respiratory chain components (Lawson et al. 2022; Wieloch et al. 2022). Recent research has highlighted the importance of understanding how plants integrate these various metabolic pathways for maintaining optimal growth in different environmental conditions (Rymen and Sugimoto 2012; Zandalinas et al. 2022). Moreover, the regulation of cellular redox status, particularly through the management of NAD(P)+/NAD(P)H ratios, emerges as a critical control point in this metabolic orchestration, affecting both energy metabolism and carbon fixation capacity (Lim et al. 2020).

A growing body of research suggests that plant metabolic adaptation to light and nutrient gradients involves intricate regulatory mechanisms that extend beyond traditional models of photosynthetic acclimation (Balcke et al. 2024; Gao et al. 2024). These adaptations might include unpredicted metabolic configurations and the coordinated regulation of divergent pathways (Fang et al. 2019; VanWallendael et al. 2019). An intriguing aspect of this metabolic plasticity is the integration of respiratory chain components with photosynthetic electron transport



Agastache rugosa (Fisch. & C.A.Mey.) Kuntze, an economically important Lamiaceae herb native to East Asia, provides a fascinating system to investigate metabolic adaptation. A. rugosa inhabits a wide ecological range, suggesting a remarkable capacity for physiological plasticity (Bielecka et al. 2019; Fonseca de Lima et al. 2021). A. rugosa also produces diverse secondary metabolites with valuable medicinal properties and commercial applications (Yamani et al. 2014; Anand et al. 2018; Kim 2020; Lee et al. 2020; Hou et al. 2022). While earlier works have explored its secondary metabolism and essential oil production (Zielińska et al. 2016; An et al. 2018; Anand et al. 2018), the underlying mechanisms of primary metabolic regulation remain poorly understood. As a non-model species, A. rugosa offers the prospect of testing the generality of plant metabolic regulation paradigms and potentially uncover distinctive strategies. Here, we examined the interactive effects of light and nutrient conditions on key parameters of photosynthetic and respiratory metabolism in A. rugosa, to elucidate novel aspects of metabolic integration. We hypothesized that A. rugosa employs distinct metabolic configurations under varying light and nutrient levels that involve: (1) differential regulation of carbon fixation pathways; (2) compensatory adjustments in respiratory metabolism; and (3) changes in cellular redox balance. By using a combination of physiological and biochemical approaches, including multivariate statistical analysis, we sought to expand the current understanding of plant metabolic adaptation and unveil new dimensions of plasticity that could further basic and applied research.

Materials and methods

Seed preparation and germination

Seeds of *Agastache rugosa* were obtained from WHT Wellgrow Seeds (Kota Damansara, Selangor, Malaysia) and underwent surface sterilization via sequential soaking in



Planta (2025) 261:133 Page 3 of 18 133

70% ethanol for 1 min followed by 5% sodium hypochlorite solution for 10 min, with three subsequent rinses using sterile distilled water. The sterilized seeds were sown in 200-cell seedling trays containing an equal-parts mixture of blonde peat and perlite. Environmental conditions during the initial growth phase were maintained using white fluorescent lighting on a 16/8 h light/dark cycle, with the temperature ranging from 20 to 25 °C and relative humidity at 50–70%. The growing medium moisture was monitored to prevent waterlogging while ensuring adequate water availability through capillary matting.

Polytunnels setup and environmental monitoring

The experimental site consisted of two north-south oriented polytunnels, each measuring $10 \text{ m} \times 6 \text{ m} \times 2 \text{ m}$, located at Farm 10, Universiti Putra Malaysia. These structures featured 1.5 m high end walls and side walls, covered with a single layer of transparent polyethylene film (280 µm thickness). The end walls remained open during the experiment, while side walls were maintained in a rolleddown position. One tunnel was modified with external 50% black shade netting on the roof to create differential light environments (Suppl. Fig. S1). Environmental monitoring was conducted using a LI-189 light meter (LI-COR, Lincoln, NE, USA) for photosynthetic photon flux density measurements (PPFD), while data loggers recorded air temperature (T_{Air}), and relative humidity (RH) during daylight hours (Suppl. Fig. S2). High-light treatment (0% shade) maintained peak PPFD values of around 1500-1700 μmol m⁻² s⁻¹ during midday, while the low-light treatment (50% shade) reached maximum values of approximately 700-800 μ mol m⁻² s⁻¹. This represents an approximately 50% reduction in light intensity, consistent with the shade netting specifications.

Experimental design and treatments

The experiment employed uniform six-week-old seedlings displaying 4–5 true leaves, which were transplanted into black polythene containers (15 cm diameter ×25 cm height) filled with 3.5 kg of 3:2:1 potting mix. The containers were laid out with 30 cm spacing between plants to ensure adequate growth space and minimize mutual shading. The experimental design incorporated four nutrient levels using NPK 16:16:16 compound fertilizer (YaraMila, Oslo, Norway); low (NPK1, 40 mg kg⁻¹, 1.26 g), moderate (NPK2, 80 mg kg⁻¹, 2.52 g), high (NPK3, 120 mg kg⁻¹, 3.78 g), and very high (NPK4, 160 mg kg⁻¹, 5.04 g), nested under two light regimes; high-light (HL, 0% shade) and low-light (LL, 50% shade). Nutrient levels were arranged in a randomized complete block design with four replications to account for

potential environmental gradients within the polytunnels and ensure statistical validity of the results.

Fertilizer applications were split across many intervals to optimize nutrient availability throughout the growth period. The initial application occurred at transplanting, with subsequent applications at 6, 13, 27, 41, 55, and 69 days after transplanting. The fertilizer was applied in 5 cm deep holes adjacent to the plants to ensure proper placement and accessibility to the root zone. Irrigation was managed using a drip system operating at a flow rate of 20 mL min⁻¹, with scheduled applications twice daily at 08:00 and 17:00 h for 15 min durations. The irrigation frequency was adjusted based on prevailing weather conditions and plant growth stage to maintain optimal soil moisture levels.

Fresh sample preparation

Fresh leaf samples (the third or the fourth from the apex) were harvested in the morning at 84 days after transplanting, flash frozen with liquid nitrogen and placed into prelabeled ziplock bags, and immediately transported to the laboratory in a cooler with ice packs. Samples were further ground with liquid nitrogen using precooled mini porcelain mortars and pestles. Powdered samples were transferred into 50 mL falcon tubes and stored in a -80 °C ultra-low temperature freezer until use (MDF-U55 V-PE, Panasonic).

Carbonic anhydrase

Carbonic anhydrase (CA, EC 4.2.1.1) activity was determined using the titration method (Wilbur and Anderson 1948; Tiwari et al. 2006) with some modifications. Frozen samples were weighed into 2 mL microtubes at 0.25 g each and homogenized with 1 mL of ice-cold extraction buffer (0.5 mM EDTA, 10 mM dithiothreitol (DTT) and 10% glycerol in 50 mM HEPES-NaOH pH 7.5). Homogenates were centrifuged at 4 °C for 10 min at 8000 g. Next, 3 mL of of ice-cold titration buffer (0.5 mM EDTA, 10 mM of DTT, 10% glycerol, and 20 ppm bromothymol blue in 50 mM HEPES-NaOH pH 8.3) and 200 µL of ice-cold deionized water were pipetted into 10 mL glass vials and vortexed for $10~\mathrm{s}.$ Then, $2~\mathrm{mL}$ of ice-cold CO_2 water (F&N Ice Mountain sparkling water) was pipetted to the mix. This commercial sparkling water was used as a standardized source of CO₂-saturated water, equivalent to the laboratory-prepared CO₂-saturated water described by Tiwari et al. (2006). The sparkling water was kept ice-cold throughout the experiment to maintain stable CO₂ concentration, and preliminary tests confirmed that the CO2 content was comparable to freshly prepared CO_2 -saturated water. The time required (T_{blank}) for the color to change from blue to yellow was recorded. The same procedure was repeated for plant extracts. In place of water, the enzyme extract was added. Ice-cold CO₂ water



133 Page 4 of 18 Planta (2025) 261:133

was pipetted at 2 mL to start the reaction. The time required (T_{sample}) for the color to change from blue to yellow was recorded. CA activity was expressed as units of CA per gram tissue fresh weight (U g⁻¹ FW) following the equation:

$$CA (U g^{-1} FW) = [(T_{blank}/T_{sample}) - 1 \times 10]/FW$$

where $T_{\rm blank}$ is the time required for blank pH to change color in min, $T_{\rm sample}$ is the time required for sample pH to change color in min, and FW is the fresh weight of sample in g.

Phosphoenolpyruvate carboxylase

Phosphoenolpyruvate carboxylase (PEPC, EC 4.1.1.31) activity was determined using an assay kit (Solarbio Science and Technology Co., Ltd., Beijing, China) by following the manufacturer's protocols. Frozen samples were weighed into 2 mL microtubes at 0.1 g each, homogenized with 1 mL of ice-cold extract solution, and centrifuged at 4 °C for 20 min at 8000 g. The supernatants were aliquoted into fresh 2 mL microtubes. Briefly, the assay protocols were as follows: For the test tubes, 20 µL of sample supernatants were added with 90 µL of Reagent I and 90 µL of working solution. The working solution was first prepared by combining Reagents II, III, IV, V, VI, and VII (15:15:15:15:19:19, by vol.). For blank tube, 90 µL of Reagent I was added with 20 uL of distilled water. The mixtures were vortexed. The first absorbance was read at 340 nm. The samples and blank were immediately incubated at 30 °C in a water bath for 5 min. The second absorbance was taken at 310 nm. PEPC activity was determined by measuring the formation of NADH using the extinction coefficient at 6220 L mol⁻¹ cm⁻¹, and expressed as units per gram tissue fresh weight (U g⁻¹ FW).

Phosphonenolpyruvate carboxykinase

Phosphonenolpyruvate carboxykinase (PEPCK, EC 4.1.1.32) activity was determined by using an assay kit (Solarbio Science and Technology Co., Ltd., Beijing, China) based on the manufacturer's protocols. Frozen samples were weighed into 2 mL microtubes at 0.1 g each, homogenized with 1 mL of ice-cold extract solution, and centrifuged at 4 °C for 20 min at 8000 g. The supernatants were added into fresh 2 mL microtubes. Briefly, the assay protocols were as follows: For the test tubes, 50 µL of sample supernatants were added with 50 µL of Reagent V and 900 µL of working solution. Working solution was first prepared by combining Reagents II, III, and IV (7:1:1, by vol.). For blank tube, 50 μL of Reagent V was added with 50 μL of distilled water and 900 µL of working solution. The mixtures were vortexed quickly after adding Reagent V. The first absorbance was read at 340 nm for 10 s. The second absorbance was taken at 70 s. PEPCK activity was determined by measuring the consumption of NADH using the extinction coefficient at $6220 \text{ L mol}^{-1} \text{ cm}^{-1}$, and expressed as units per gram tissue fresh weight (U g⁻¹ FW).

Pyruvate dehydrogenase complex

Pyruvate dehydrogenase complex (PDC) activity was determined using the spectrometric method with modifications (Thiellement 2010; Huang et al. 2015). Briefly, frozen samples were weighed into 15 mL falcon tubes at 0.5 g each, and homogenized with 10 mL of icecold homogenization buffer (0.4 M mannitol, 5 mM EGTA, 10 mM L-cysteine, 0.5% BSA, and 1% PVP-40 in 50 mM sodium pyrophosphate–KOH pH 7.8). Homogenates were filtered through two layers of nonwoven gauze, with a gentle hand pressure being applied in order to increase the final crude mitochondrial yield. The filtrates were then centrifuged at 4 °C for 5 min at 1500 g. The supernatants containing mitochondrial suspensions were transferred into fresh 15 mL falcon tubes and centrifuged at 4 °C for 15 min at 18,000 g; the resulting supernatants were discarded. Pellets were resuspended in 2 mL of resuspending buffer (0.3 M mannitol and 0.1% BSA in 10 mM TES-KOH pH 7.2) by gently swirling the tubes. After discarding the supernatants, the pellets were washed again with 2 mL of resuspending buffer. This step was repeated three times. After the final washing, the pellets were resuspended in 300 μL of resuspending buffer and stored under -80 °C until analyses. For the PDC assay, 980 µL of reaction medium (0.2% Triton X-100, 1 mM β–NAD⁺, 1 mM MgCl₂, 0.2 mM thiamine pyrophosphate, 0.12 mM lithium-CoA, 2 mM L-cysteine, and 1 mM sodium pyruvate in 50 mM sodium TES-NaOH pH 7.6) was pipetted into 2 mL microtubes and added with 20 µL of mitochondrial suspensions. The mixtures were vortexed and incubated at 35 °C in a water bath for 3 min. Absorbance was read at 340 nm before and after incubation. PDC activity was determined by measuring the formation of NADH using the extinction coefficient at 6220 L mol⁻¹ cm⁻¹, and expressed as picokatal per gram tissue fresh weight (pkatal g⁻¹ FW). One unit of activity (katal) is defined as the amount of PDC catalyzing the formation of 1 mol NADH in 1 s.

NADH-UQ oxidoreductase

NADH–ubiquinone oxidoreductase (NADH–UQ, EC 1.6.5.3) activity was determined using the spectrometric method with modifications (Thiellement 2010; Huang et al. 2015). Briefly, 980 μ L of reaction medium (50 mM sodium chloride, 0.2 mM NADH, and 1 mM ferricyanide in 50 mM Tris–HCL pH 7.2) and 20 μ L of the prepared mitochondrial suspensions were pipetted into 2 mL microtubes. After



Planta (2025) 261:133 Page 5 of 18 **133**

vortexing and incubating at 35 °C in a water bath for 3 min, absorbance was read at 420 nm before and after incubation. NADH:UQ activity was determined by measuring NADH reduction of ferricyanide using the extinction coefficient at 0.00103 L mol⁻¹ cm⁻¹, and expressed as millikatals per gram tissue fresh weight (mkatal/g FW). One unit of activity (katal) is defined as the amount of NADH catalyzing the reduction of 1 mol ferricyanide in 1 s.

Cytochrome c oxidase

Cytochrome c oxidase (COX, EC 7.1.1.9) activity was determined using the spectrometric method with modifications (Thiellement 2010; Huang et al. 2015). Briefly, 980 μ L of reaction medium (0.05 mM reduced cytochrome c in 21 mM potassium phosphate buffer pH 7.4) and 20 μ L of the mitochondrial suspensions were pipetted into 2 mL microtubes. After vortexing and incubating at 35 °C in a water bath for 3 min, absorbance was read at 550 nm before and after incubation. COX activity was determined by measuring cytochrome c oxidation using the extinction coefficient at 28 L mol⁻¹ cm⁻¹, and expressed as nanokatals per gram tissue fresh weight (nkatal/g FW). One unit of activity (katal) is defined as the amount of cytochrome c oxidase oxidizing 1 mol of cytochrome c in 1 s.

NADP+/NADPH

Nicotinamide adenine dinucleotide phosphate (NADP⁺) and the reduced NADP⁺ (NADPH) contents, and their ratio were determined using the Coenzyme II NADP(H) assay kit (Solarbio Science and Technology Co., Ltd., Beijing, China) following the manufacturer's protocols. To extract NADP⁺, frozen samples were weighed into 2 mL microtubes at 0.1 g each and homogenized with 1 mL of acid extract solution. The homogenates were incubated in a water bath at 95 °C for 5 min, left to cool, and then centrifuged for 10 min at 10,000 g. The supernatants were aliquoted into fresh 2 mL microtubes at 500 µL each and pipetted with equal volume of alkaline extract solution. After vortexing and centrifuging for 10 min at 10,000 g, the supernatants were transferred into 2 mL microtubes. To extract NADPH, frozen samples were weighed into 2 mL microtubes at 0.1 g each and homogenized with 1 mL of alkaline extract solution. The homogenates were incubated in a water bath at 95 °C for 5 min, left to cool, and centrifuged for 10 min at 10,000 g. The supernatants were aliquoted into fresh 2 mL microtubes at 500 µL each and pipetted with equal volume of acid extract solution. After vortexing and centrifuging for 10 min at 10,000 g, the supernatants were transferred into fresh 2 mL microtubes.

Briefly, the assay protocols were as follows: For the test tubes, 50 µL of sample supernatants were pipetted. For the

control tubes, 50 μ L of sample supernatants were pipetted with 500 μ L of Reagent VI. The mixtures were pipetted with 250 μ L of Reagent I, 75 μ L of Reagent II, 75 μ L of Reagent III, 75 μ L of Reagent IV, and 35 μ L of Reagent V. The mixtures were vortexed and incubated for 20 min at room temperature (20–25 °C) in the dark. Next, 500 μ L of Reagent VI was pipetted to the test tubes. The mixtures were vortexed, left to stand for 5 min, and centrifuged for 5 min at 20,000 g. After discarding the supernatants, the pellets were suspended in 1 mL of Reagent VII. Absorbance was read at 570 nm. NADP⁺ and NADPH contents were expressed as nanomoles per gram tissue fresh weight (nmol g⁻¹ FW), while their ratios were calculated by dividing the obtained values.

NAD+/NADH

Nicotinamide adenine dinucleotide (NAD⁺) and the reduced NAD+ (NADH) contents, and their ratio were determined using the NAD(H) assay kit (Solarbio Science and Technology Co., Ltd., Beijing, China) according to the manufacturer's protocols. To extract NAD⁺, frozen samples were weighed into 2 mL microtubes at 0.1 g each and homogenized with 0.5 mL of ice-cold acid extract solution. The mixtures were boiled for 5 min and left to cool. The homogenates were centrifuged at 4 °C for 10 min at 10,000 g. The supernatants were aliquoted into fresh 2 mL microtubes at 200 µL each and pipetted with equal volume of ice-cold alkaline extract solution. The mixtures were vortexed and centrifuged at 4 °C for 10 min at 10,000 g. The supernatants were transferred into fresh 2 mL microtubes. For NADH extraction, frozen samples were weighed into 2 mL microtubes at 0.1 g each and homogenized with 0.5 mL of ice-cold alkaline extract solution. The mixtures were boiled for 5 min and left to cool. The homogenates were then centrifuged at 4 °C for 10 min at 10,000 g. The supernatants were aliquoted into fresh 2 mL microtubes at 200 μL each and added with equal volume of ice-cold acid extract solution. The mixtures were vortexed and centrifuged at 4 °C for 10 min at 10,000 g. The supernatants were transferred into fresh 2 mL microtubes.

Briefly, the assay protocols were as follows: For the test tubes, $50~\mu L$ of sample supernatants were pipetted. For the control tubes, $50~\mu L$ of sample supernatants were pipetted with $500~\mu L$ of Reagent VI. For the standard tubes, $50~\mu L$ of NAD or NADH standards were pipetted. For the blank tube, $50~\mu L$ of distilled tube was pipetted. The mixtures were pipetted with $250~\mu L$ of Reagent II, $75~\mu L$ of Reagent III, $75~\mu L$ of Reagent IV, and $35~\mu L$ of Reagent V. The mixtures were vortexed and incubated for 20~min at room temperature ($20-25~^{\circ}C$) in the dark. Next, $500~\mu L$ of Reagent VI was pipetted to the test, standard,



133 Page 6 of 18 Planta (2025) 261:133

and blank tubes. The mixtures were vortexed, left to stand for 5 min, and then centrifuged for 5 min at 20,000 g. After discarding the supernatants, the pellets were resuspended in 1 mL of Reagent VII. Absorbance was read at 570 nm. NAD⁺ and NADH contents were expressed as nanomoles per gram tissue fresh weight (nmol g⁻¹ FW), while their ratios were calculated by dividing the obtained values.

Adenosine triphosphate

Adenosine triphosphate (ATP) content was determined using an assay kit (Solarbio Science and Technology Co., Ltd., Beijing, China) following the manufacturer's protocols. Frozen samples were weighed into 2 mL microtubes at 0.1 g each, and homogenized with 1 mL of ice-cold extract solution. The homogenates were centrifuged at 4 °C for 10 min at 10,000 g. The supernatants were transferred into fresh 2 mL microtubes, pipetted with 500 µL chloroform, and vortexed. Samples were centrifuged at 4 °C for 3 min at 10,000 g. Briefly, the assay protocols were as follows: For the test tubes, 100 µL of sample supernatants were pipetted with 640 μL of Reagent I and 260 μL of working solution. The working solution was prepared by combining Reagents II, III, IV, V, and VI (1:1:0.1:0.4:0.1, by vol.). For the standard tubes, 100 µL of standard solution was pipetted with 640 µL of Reagent I and 260 µL of the working solution. The 10 μ mol mL⁻¹ standard solution was first diluted to 0.625 µmol mL⁻¹ with distilled water. The mixtures were vortexed and incubated for 3 min at room temperature (20–25 °C). Absorbance was read at 340 nm before and after incubation. ATP content was expressed as micromoles per gram tissue fresh weight (µmol g⁻¹ FW).

Statistical analysis

Data were analyzed using SAS® version 9.4 by the general linear model (PROC GLM). Wherever necessary, data was transformed before analysis through Box-Cox transformations to ensure the normality of residuals was satisfied. A combined analysis of variance (ANOVA) was performed for the four nutrient levels nested under light treatments (Bowley 1999; Moore and Dixon 2015). The ANOVA of the combined analysis considered the fixed effects for light, replication, nutrient, and interaction between light and nutrient. The means of significant main effects and interactions (P < 0.05) were separated with least significant difference (LSD) posthoc test (Vargas et al. 2015). For multivariate analyses, data were standardized to zero mean and unit variance. We further used Pearson's correlation test, principal component analysis (PCA), and hierarchical

cluster analysis (HCA) to explore the relationship among variables and group them based on their similarities. For HCA, we used the furthest neighbor (complete linkage) clustering method with correlation distance to identify relationships between metabolic parameters. Graphs, heatmap, dendrogram, and PCA biplot were made using OriginPro® 2024b.

Results

Carbon fixation

Interaction effect (P < 0.05) was observed between light and nutrient levels on carbonic anhydrase (CA) activity in A. rugosa (Fig. 1). CA activity exhibited a distinct peak under HL–NPK2 (5.17 ± 0.26 U g⁻¹ FW), while consistently lower activities were observed under low-light levels across all nutrient treatments. The response to nutrient levels followed a clear pattern, where low (NPK1) and higher nutrients (NPK3 and NPK4) led to significant decreases in CA activity, regardless of light conditions. This trend was particularly drastic in the low-light treatment, culminating in the lowest observed CA activity under LL–NPK4 (0.51 ± 0.05 U g⁻¹ FW), representing a substantial 90.1% reduction from the peak activity.

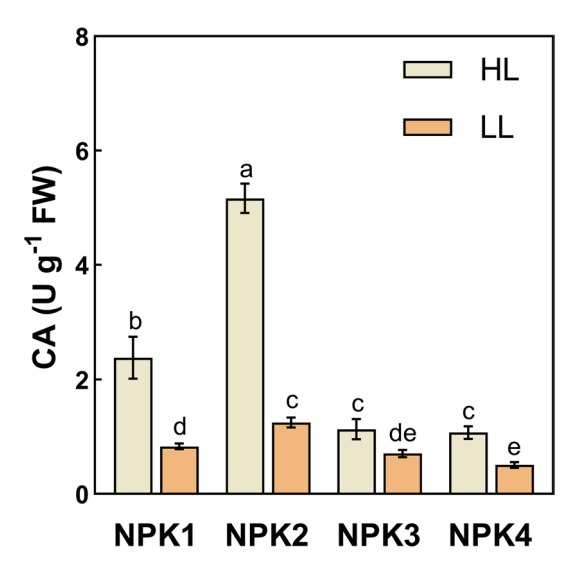
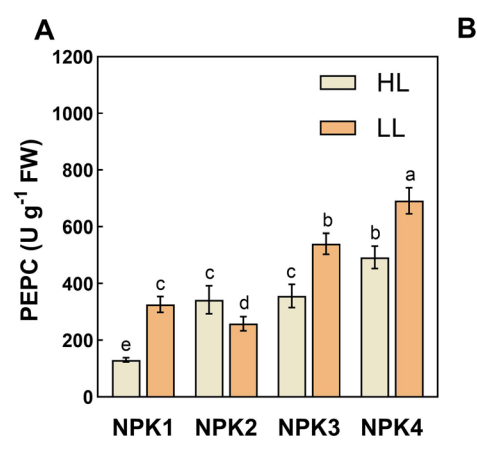
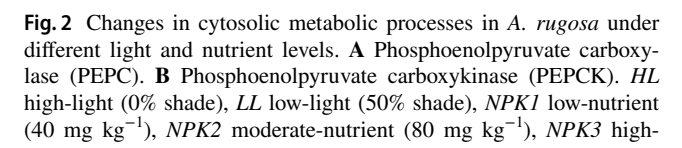


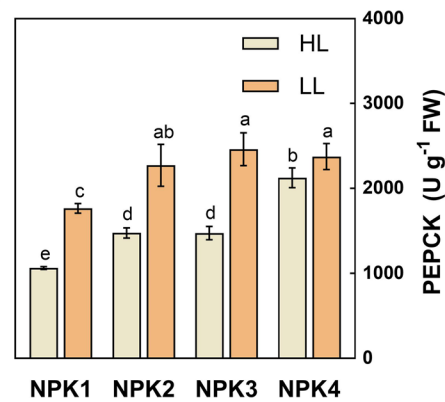
Fig. 1 Changes in carbonic anhydrase (CA) activity in *A. rugosa* under different light and nutrient levels. *HL* high-light (0% shade), *LL* low-light (50% shade), *NPK1* low-nutrient (40 mg kg⁻¹), *NPK2* moderate-nutrient (80 mg kg⁻¹), *NPK3* high-nutrient (120 mg kg⁻¹), *NPK4* very high-nutrient (160 mg kg⁻¹). Mean values \pm SD (n = 4). Different letter(s) above bars indicate significant differences according to LSD (least significant difference)



Planta (2025) 261:133 Page 7 of 18 133







nutrient (120 mg kg⁻¹), *NPK4* very high-nutrient (160 mg kg⁻¹). Mean values \pm SD (n=4). Different letter(s) above bars indicate significant differences according to LSD (least significant difference)

Anaplerotic metabolism

Light and nutrient showed significant interaction effects (P < 0.05) on PEPC and PEPCK activities in A. rugosa under different light and nutrient levels (Fig. 2). PEPC activity in high-light adapted plants exhibited progressive increases with nutrient levels, from NPK1 (130.72 \pm 7.49 U g⁻¹ FW) to NPK4 (492.74 \pm 39.32 U g⁻¹ FW; 276.9% increase). The low-light treatment resulted in elevated PEPC activities across nutrient levels, with NPK2 (258.41 \pm 24.96 U g^{-1} FW) and NPK4 (691.67 \pm 46.08 U g^{-1} FW; averaging 110.7% increase) showing the minimum and maximum values, respectively (Fig. 2A). PEPCK activity displayed distinct responses under different light conditions. At highlight levels, PEPCK activity increased from NPK1 (1064.98 $\pm 17.57 \text{ U g}^{-1} \text{ FW}$) through NPK2 (1477.53 $\pm 60.62 \text{ U g}^{-1}$ FW; 38.7% increase) and NPK3 (1475.97 \pm 79.17 U g⁻¹ FW; 38.6% increase), reaching its peak at NPK4 (2124.49 ±115.69 U g⁻¹ FW; 99.5% increase). Low-light treatments maintained higher PEPCK activities throughout all nutrient levels, beginning at NPK1 (1768.20 \pm 55.52 U g⁻¹ FW) and showing consistently elevated values across NPK2-NPK4 treatments (averaging 2369.84 \pm 197.30 U g⁻¹ FW; 34.3% increase) (Fig. 2B).

Mitochondrial metabolic processes

Interaction and independent effects (P < 0.05) were observed between light and nutrient levels on mitochondrial metabolic processes in *A. rugosa* (Fig. 3). PDC activity under highlight conditions showed a decreasing trend with increasing nutrient levels, declining from NPK1 (251.79 \pm 40.12 nkatal g⁻¹ FW) through NPK2 (147.55 \pm 13.23 nkatal g⁻¹

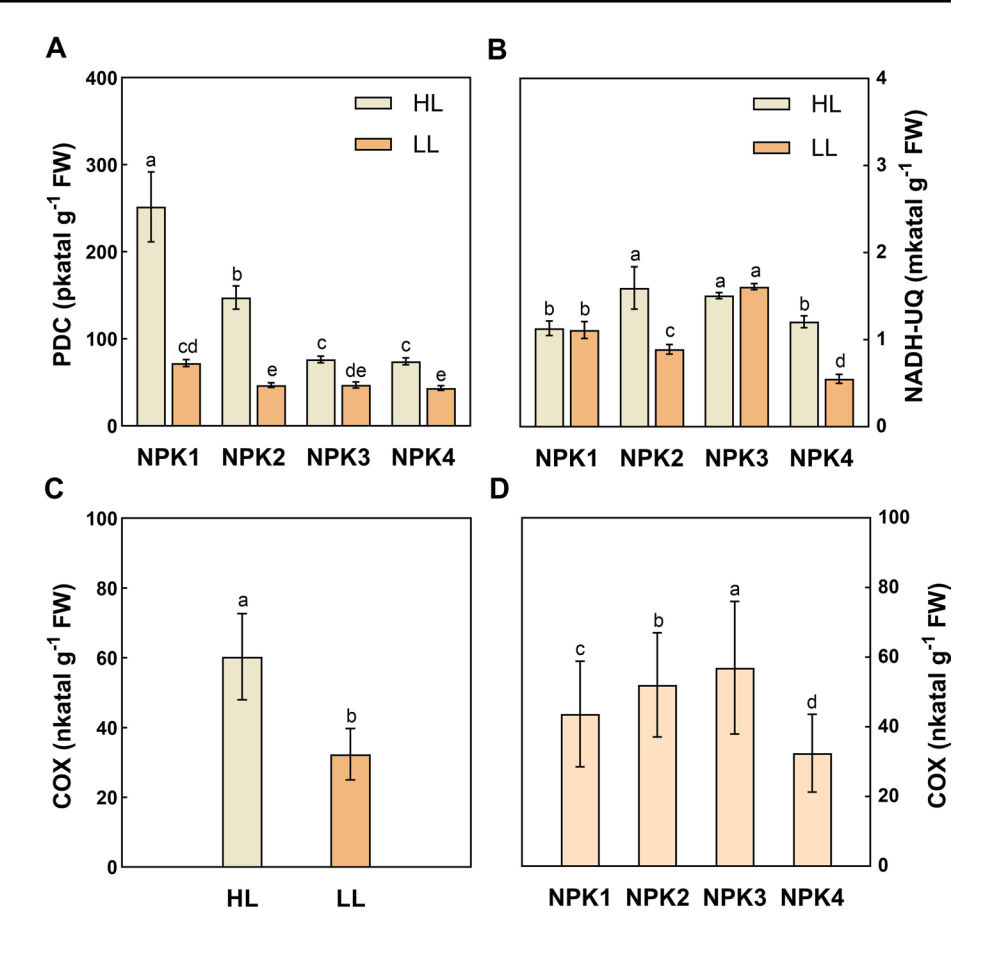
FW; 41.4% decrease), NPK3 (76.37 \pm 3.89 nkatal g⁻¹ FW; 69.7% decrease) to NPK4 (74.13 \pm 3.93 nkatal g⁻¹ FW; 70.6% decrease). Low-light levels consistently exhibited lower PDC activities, ranging from NPK1 (72.17 ± 4.10 nkatal g^{-1} FW) to NPK4 (43.41 \pm 2.65 nkatal g^{-1} FW; 39.9% decrease) (Fig. 3A). NADH-UQ activity demonstrated different patterns between light treatments across nutrient levels. Under high-light conditions, values ranged from NPK1 (1.13 ± 0.08 mkatal g⁻¹ FW) to NPK4 (1.21 ± 0.07 mkatal g⁻¹ FW; 7.1% increase), with peaks observed at NPK2 and NPK3. Low-light conditions showed a different pattern, with activity decreasing from NPK1 (1.11 $\pm 0.10 \text{ mkatal g}^{-1} \text{ FW}$) to NPK4 (0.55 $\pm 0.05 \text{ mkatal g}^{-1}$ FW; 50.5% decrease). Both light treatments showed similar NADH-UQ activity at NPK1, but increasingly diverged as nutrient levels increased, with significant reduction in activity observed at NPK4 under low-light conditions (Fig. 3B). COX activity showed marked differences between light conditions (HL: 60.30 ± 12.37 nkatal g⁻¹ FW; LL: 32.34 ± 7.36 nkatal g⁻¹ FW; 46.4% decrease) (Fig. 3C). Across nutrient levels, COX activity increased from NPK1 (43.72 \pm 15.17 nkatal g^{-1} FW) through NPK2 (52.08 \pm 14.98 nkatal g^{-1} FW; 19.1% increase) and NPK3 (55.99 \pm 19.07 nkatal g⁻¹ FW; 28.1% increase), followed by a significant decline in NPK4 (32.49 \pm 11.17 nkatal g⁻¹ FW; 25.7% decrease from NPK1) (Fig. 3D).

Redox balance

Light and nutrient showed interaction and independent effects (P < 0.05) on redox balance status in A. rugosa (Fig. 4). NADP⁺ contents differed between light treatments, with high-light conditions yielding higher levels (292.18



Fig. 3 Changes in mitochondrial metabolic processes in A. rugosa under different light and nutrient levels. A Pyruvate dehydrogenase complex (PDC). B NADH-ubiquinone oxidoreductase (NADH-UQ). C, D Cytochrome c oxidase (COX). HL high-light (0% shade), LL low-light (50% shade), NPK low-nutrient (40 mg kg^{-1}), NPK2 moderate-nutrient (80 mg kg^{-1}), NPK3 high-nutrient (120) mg kg⁻¹), NPK4 very highnutrient (160 mg kg⁻¹). Mean values \pm SD (n = 4). Different letter(s) above bars indicate significant differences according to LSD (least significant difference)



 ± 9.36 nmol g⁻¹ FW) compared to low-light (235.80 ± 14.69 nmol g⁻¹ FW; 19.3% decrease) (Fig. 4A). NADP⁺ contents remained relatively consistent across NPK1 through NPK3 treatments ($\sim 260 \pm 25 \text{ nmol g}^{-1} \text{ FW}$) but exhibited a significant decline in NPK4 (255.25 ± 40.03 nmol g⁻¹ FW; 5% decrease) (Fig. 4B). NADP+/NADPH ratio displayed markedly higher values under high-light conditions (1.07 \pm 0.05) compared to low-light (0.85 \pm 0.05; 20.6% decrease), indicating substantial differences in the redox state between light treatments (Fig. 4C). Notably, light and nutrient did not affect (P > 0.05) NADPH content in A. rugosa (Table 1). NAD⁺ content exhibited a nutrient-dependent reduction from NPK1 (2.83 \pm 0.22 nmol g⁻¹ FW) to NPK4 (2.43 \pm 0.14 nmol g⁻¹ FW; 14.1% decrease) (Fig. 4D), while NADH content showed significant differences between light treatments (HL: $3.51 \pm 0.17 \text{ nmol g}^{-1}$ FW; LL: $3.17 \pm 0.18 \text{ nmol g}^{-1}$ FW; 9.7% decrease) (Fig. 4E). The NAD+/NADH ratio was higher under high-light conditions (0.86 \pm 0.10) compared to low-light levels (0.75 \pm 0.06; 12.8% decrease) (Fig. 4F), with an overall decline across nutrient treatments from NPK1 (0.84 ± 0.07) to NPK4 $(0.74 \pm 0.07; 11.9\%)$ decrease) (Fig. 4G).

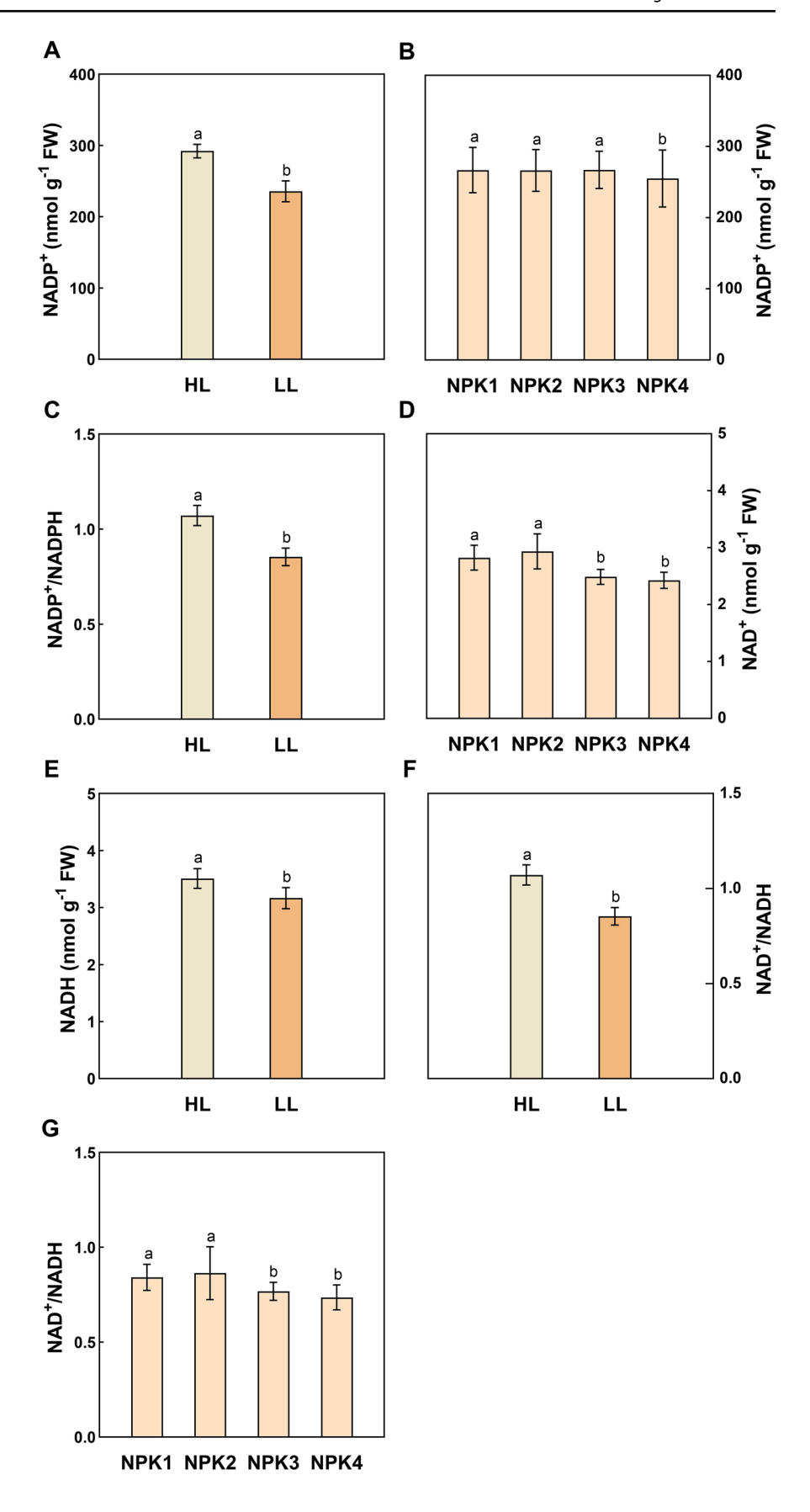
ATP homeostasis

Light and nutrient demonstrated significant interaction effects (P < 0.05) on ATP accumulation in A. rugosa under different light and nutrient levels (Fig. 5). Under high-light conditions, ATP levels remained consistently low across all nutrient treatments (NPK1: 1.45 ± 0.09 ; NPK2: 1.77 ± 0.06 ; NPK3: 1.27 ± 0.11 ; NPK4: 1.24 ± 0.10 nmol g⁻¹ FW), demonstrating no significant variations. In contrast, low-light plants exhibited markedly higher ATP concentrations with significant nutrient-dependent variations. The highest ATP content in low-light plants was observed in NPK3 (12.88 $\pm 0.84 \text{ nmol g}^{-1} \text{ FW}$), followed by NPK1 (11.61 ± 0.85 nmol g⁻¹ FW; 9.9% decrease), while NPK2 showed substantially lower concentrations (7.02 \pm 0.49 nmol g⁻¹ FW; 45.5% decrease from peak). The lowest ATP content in lowlight conditions was recorded in NPK4 (4.61 \pm 0.13 nmol g⁻¹ FW), indicating a 64.2% decrease from the peak value observed in NPK3. The difference between high-light and low-light conditions was most pronounced at NPK3, where low-light ATP contents were 90.1% higher than the corresponding high-light treatment.



Planta (2025) 261:133 Page 9 of 18 **133**

Fig. 4 Changes in redox balance status in A. rugosa under different light and nutrient levels. A, B Nicotinamide adenine dinucleotide phosphate (NADP⁺). C NADP⁺ to reduced NADP+ ratio (NADP+/ NADPH). D Nicotinamide adenine dinucleotide (NAD+). E Reduced nicotinamide adenine dinucleotide (NADH). F, G NAD+ to reduced NAD+ ratio (NAD+/NADH). HL high-light (0% shade), LL low-light (50% shade), NPK low-nutrient (40 mg kg⁻¹), NPK2 moderatenutrient (80 mg kg⁻¹), NPK3 high-nutrient (120 mg kg⁻¹), NPK4 very high-nutrient (160 mg kg⁻¹), Mean \pm SD (n = 4). Different letter(s) above bars indicate significant differences according to LSD (least significant difference)





133 Page 10 of 18 Planta (2025) 261:133

Table 1 Independent effects of light and nutrient on reduced nicotinamide adenine dinucleotide phosphate (NADPH) concentrations in *A. rugosa*

Treatments		NADPH (nmol g ⁻¹ FW)
Light	HL	272.81 ± 6.01^{a}
	LL	276.23 ± 13.09^{a}
Nutrient	NPK1	274.88 ± 7.06^{a}
	NPK2	276.69 ± 3.83^{a}
	NPK3	277.26 ± 6.82^{a}
	NPK4	269.25 ± 17.36^{a}
F value	Light (L)	NS
	Nutrient (N)	NS
	LxN	NS

Mean values \pm SD (n= 4). Means within the same column followed by the different letter(s) were significantly different according to LSD (least significant difference)

HL high-light (0% shade), LL low-light (50% shade), NPK1 low-nutrient (40 mg $\rm kg^{-1}),$ NPK2 moderate-nutrient (80 mg $\rm kg^{-1}),$ NPK3 high-nutrient (120 mg $\rm kg^{-1}),$ NPK4 very high-nutrient (160 mg $\rm kg^{-1}),$ NS not significant

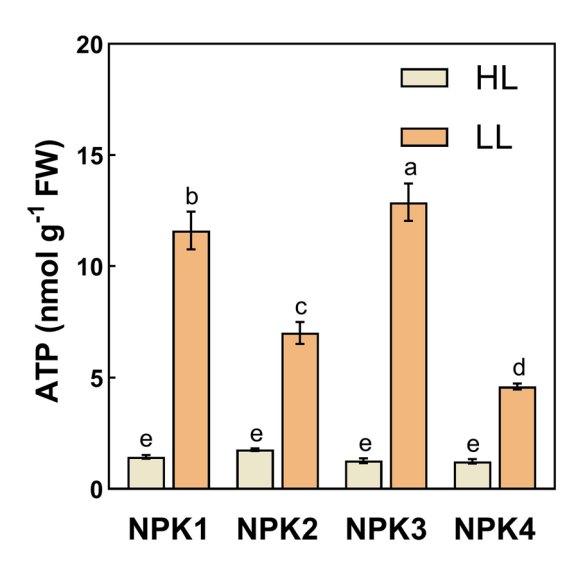


Fig. 5 Changes in adenosine triphosphate (ATP) production and utilization in *A. rugosa* under different light and nutrient levels. *HL* highlight (0% shade), *LL* low-light (50% shade), *NPK1* low-nutrient (40 mg kg⁻¹), *NPK2* moderate-nutrient (80 mg kg⁻¹), *NPK3* high-nutrient (120 mg kg⁻¹), *NPK4* very high-nutrient (160 mg kg⁻¹), Mean \pm SD (n=4). Different letter(s) above bars indicate significant differences according to LSD (least significant difference)

Correlations among measured traits

The heatmap reveals complex relationships between metabolic traits in *A. rugosa* under varying light and nutrient levels (Fig. 6). The highest positive correlation was observed between NADP⁺ and NADP⁺/NADPH (r = 0.96, P < 0.001),

while both showed strong positive correlations with COX (r = 0.81 and 0.74, respectively, P < 0.001) and moderate negative correlations with ATP (r = -0.67 and -0.69, respectively, P < 0.001). PDC showed strong negative correlations with PEPCK (r = -0.81, P < 0.001), while showing positive correlations with NADP⁺ (r = 0.64, P < 0.001), and NADP⁺/ NADPH (r = 0.65, P < 0.001). The NAD⁺/NADH ratio demonstrated significant positive correlations with NAD⁺ (r = 0.79, P < 0.001), CA (r = 0.76, P < 0.001), and PDC (r = 0.63, P < 0.001). PEPCK showed strong positive correlations with PEPC (r = 0.71, P < 0.001), while negatively correlating with COX (r = -0.71, P < 0.001) and NADP⁺ (r = -0.67, P < 0.001). NADH-UQ demonstrated moderate positive correlations with COX (r = 0.68, P < 0.001) and NADP⁺ (r = 0.58, P < 0.001), while ATP showed largely negative correlations with most traits, with the strongest observed with NADP+/NADPH (r = -0.69, P < 0.001) and NADP⁺ (r = -0.67, P < 0.001), and moderate positive correlation with NADH (r = 0.55, P < 0.01).

Principal component analysis of selected traits

Principal component analysis (PCA) of metabolic traits in A. rugosa exposed to different light and nutrient conditions accounted for 71.2% of total variance, with Dim1 explaining 55.5% and Dim2 accounting for 15.7% (Fig. 7). The vectors CA, PDC and NAD+/NADH showed strong positive loadings on Dim1 with acute angles between them (< 45°), clustering primarily with high-light treatments (HL-NPK1-4). NADP⁺, NADP⁺/NADPH, and COX also loaded positively on Dim1 but with broader angles (60–75°) relative to the first group. PEPC, and PEPCK displayed strong negative loadings on both dimensions, with almost parallel vector angles (< 30°) associating with low-light treatments (LL–NPK1–4). Meanwhile, NADH and ATP showed strong positive loadings on Dim2 and nearly perpendicular angles (80–90°) to the Dim1 vectors. NADH-UQ demonstrated moderate negative loading on Dim2. The scatter plot also revealed distinct treatment groupings: HL-NPK1 and HL-NPK2 samples clustered in the positive region of Dim1, HL-NPK3 and HL-NPK4 samples grouped in the negative region of Dim2, while LL-NPK1 and LL-NPK2 samples located in the positive region of Dim2. LL-NPK3 and LL-NPK4 samples were distributed across the negative regions of both dimensions.

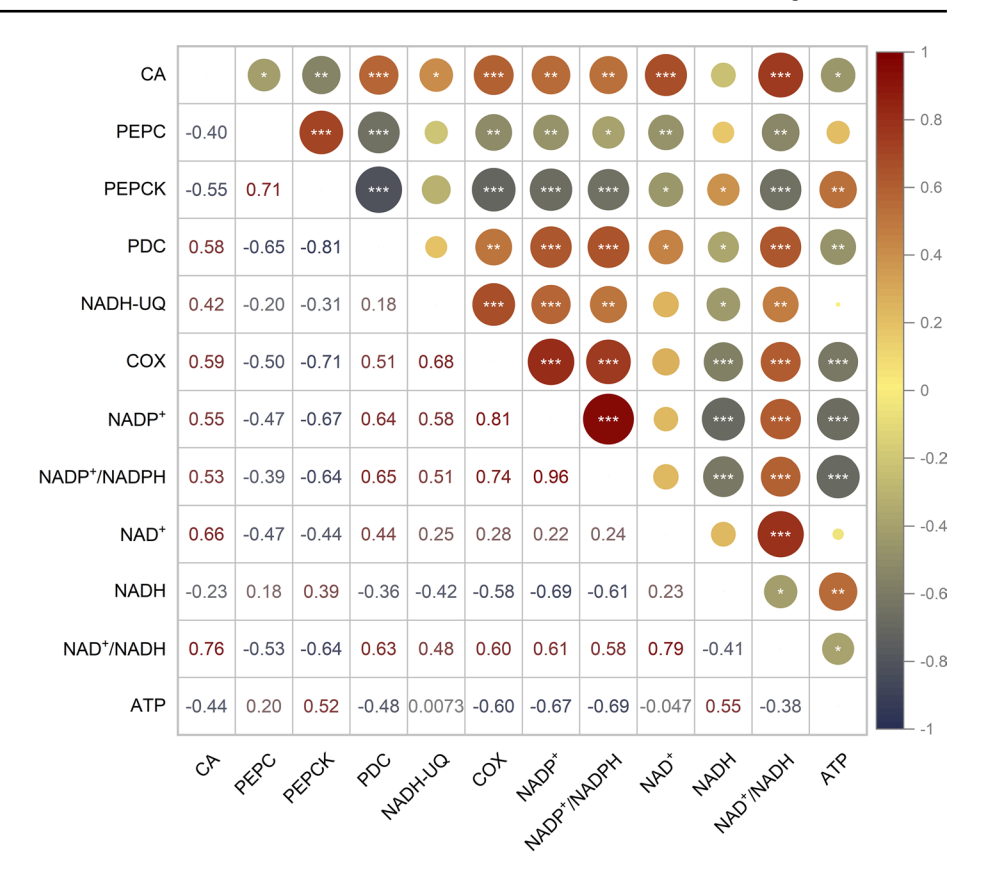
Cluster analysis of selected traits

Hierarchical clustering analysis (HCA) of metabolic traits in *A. rugosa* first bifurcated at > 50% similarity into two major clusters representing distinct light-dependent responses (Fig. 8). The first major branch encompassed traits predominantly associated with high-light treatments, including PDC, CA, NAD⁺, NAD⁺/NADH, NADP⁺, NADP⁺/NADPH,



Planta (2025) 261:133 Page 11 of 18 **133**

Fig. 6 Heatmap showing correlations between selected traits connected to metabolic reprogramming in A. rugosa at different light and nutrient levels. CA carbonic anhydrase, PEPC phosphoenolpyruvate carboxylase, PEPCK phosphoenolpyruvate carboxykinase, PDC pyruvate dehydrogenase complex, NADH-UO NADH-ubiquinone oxidoreductase, COX cytochrome c oxidase, NADP+ nicotinamide adenine dinucleotide phosphate, NADPH reduced nicotinamide adenine dinucleotide phosphate, NAD⁺ nicotinamide adenine dinucleotide, NADH reduced nicotinamide adenine dinucleotide, ATP adenosine triphosphate (***P< 0.001; **P< 0.01; *P < 0.05)



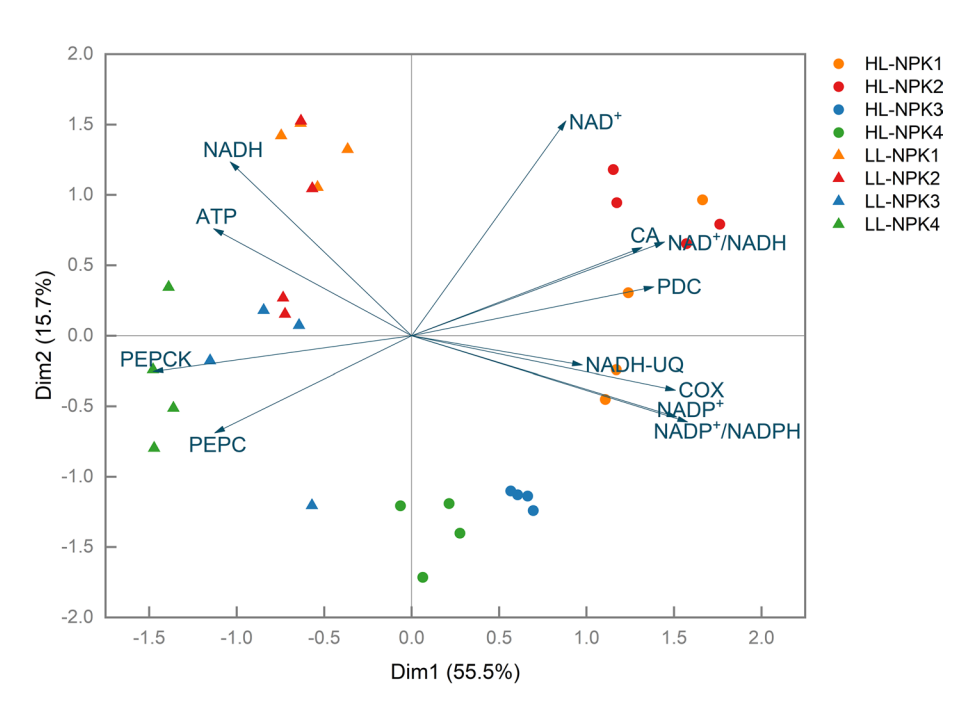


Fig. 7 Principal component analysis biplot showing the relationship among selected traits related to metabolic reprogramming in *A. rugosa* under different light and nutrient levels. *HL* high-light (0% shade), *LL* low-light (50% shade), *NPK* low-nutrient (40 mg kg⁻¹), *NPK2* moderate-nutrient (80 mg kg⁻¹), *NPK3* high-nutrient (120 mg kg⁻¹), *NPK4* very high-nutrient (160 mg kg⁻¹), *CA* carbonic anhydrase, *PEPC* phosphoenolpyruvate carboxylase, *PEPCK* phospho-

enolpyruvate carboxykinase, PDC pyruvate dehydrogenase complex, NADH-UQ NADH-ubiquinone oxidoreductase, COX cytochrome c oxidase, $NADP^+$ nicotinamide adenine dinucleotide phosphate, NADPH reduced nicotinamide adenine dinucleotide phosphate, NAD^+ nicotinamide adenine dinucleotide, NADH reduced nicotinamide adenine dinucleotide, ATP adenosine triphosphate



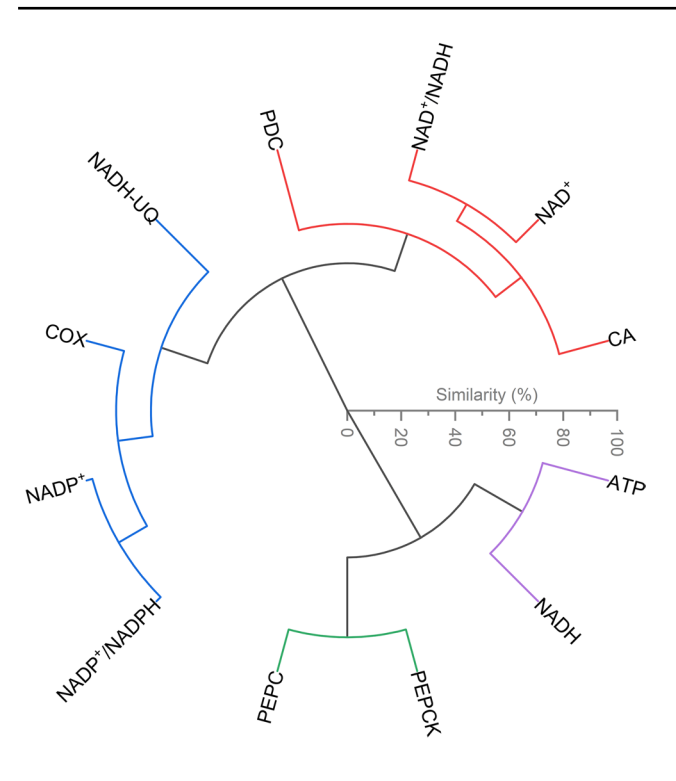


Fig. 8 Cluster analysis of selected traits related to metabolic reprogramming in *A. rugosa* under different light and nutrient levels. *CA* carbonic anhydrase, *PEPC* phosphoenolpyruvate carboxylase, *PEPCK* phosphoenolpyruvate carboxylase, *PEPCK* phosphoenolpyruvate carboxylase, *PDC* pyruvate dehydrogenase complex, *NADH–UQ* NADH–ubiquinone oxidoreductase, *COX* cytochrome c oxidase, *NADP*⁺ nicotinamide adenine dinucleotide phosphate, *NADPH* reduced nicotinamide adenine dinucleotide phosphate, *NADP* nicotinamide adenine dinucleotide, *NADH* reduced nicotinamide adenine dinucleotide nicotinamide adenine dinucleotide, *NADH* reduced nicotinamide adenine dinucleotide phosphate. The traits connected to the circular lines indicate that they have high similarity and are aggregated. The colored lines represent the four groups of clustering analysis results. Different colors are only used to better distinguish the four groups

COX, and NADH-UQ, which further subdivided (> 70% similarity). Within this high-light branch, PDC, CA, NAD⁺, and NAD+/NADH ratio formed a tight cluster (> 60% similarity) showing positive loadings on the PCA biplot Dim1, while NADP+, NADP+/NADPH, COX, and NADH-UQ grouped separately with negative loadings on Dim2. The second major branch comprised traits associated with lowlight levels, segregating into two distinct clusters (> 75% similarity), one containing PEPC, and PEPCK (~ 80% similarity) displaying strong negative loadings on both PCA dimensions, and another comprising NADH and ATP (~ 79% similarity) showing strong positive loadings on Dim2. This hierarchical organization was distinctly supported by the PCA biplot, where the spatial distribution of traits reflected their physiological relations in different light conditions, with clear separation between high-light and low-light metabolic responses.



The metabolic reprogramming observed in *A. rugosa* under varying light and nutrient conditions uncovers a remarkable capacity for physiological plasticity that challenges several conventional paradigms of plant responses to environmental factors. The most striking finding was the distinct metabolic strategies employed by *A. rugosa* under high-light versus low-light conditions. Rather than simply downregulating photosynthesis under light limitation as might be expected, low-light adapted plants showed a compensatory mechanism involving the coordinated upregulation of key enzymes across multiple carbon fixation pathways.

Under high-light conditions, A. rugosa showed a contrasting suite of metabolic adaptations geared towards optimizing photosynthetic efficiency and sustaining redox homeostasis. High-light plants demonstrated significant enhancements in carbonic anhydrase (CA) activity compared to low-light plants. This light-dependent enhancement of CA activity aligns with findings by Burnell et al. (1990), who reported that CA activity in maize leaves increased by over 100-fold in illuminated leaves and decreased in leaves placed in darkness. CA enables the interconversion of CO₂ and HCO₃⁻, effectively increasing the concentration of CO₂ around Rubisco active sites (DiMario et al. 2017). Notably, our study represents the first report examining CA activity under interactive effects of both light regimes and varying NPK nutrient levels, revealing distinct response patterns not previously documented. CA activity peaked under high-light and moderate-nutrient treatment (HL-NPK2, 5.17 ± 0.26 U g⁻¹ FW), indicating an ideal balance point where the benefits of higher CO₂ supply are maximized without unduly sacrificing nitrogen resources that could otherwise be allocated to the photosynthetic machinery. Interestingly, CA activity at low-nutrient levels (HL-NPK1) remained higher than at high-nutrient levels (HL-NPK3 and HL-NPK4), suggesting a non-linear response to nutrient availability. Under nutrient limitation, A. rugosa appears to prioritize carbon acquisition mechanisms, including maintaining relatively high CA activity, to compensate for restricted growth potential (Stitt and Krapp 1999; Trugman and Anderegg 2025), while under nutrient abundance, the plant diverts resources away from carbon acquisition towards nitrogen assimilation and growth processes (Nunes-Nesi et al. 2010). While previous studies have shown CA activity was reduced in plants grown under declining nitrogen availability (Burnell et al. 1990; Mohammad et al. 1998), our results reveal a more complex relationship where both insufficient and excessive nutrient conditions diminish CA activity in A. rugosa, with an optimal response at moderate NPK levels. Furthermore, the concurrent maintenance of a more oxidized cellular redox state at high-light and moderate-nutrient levels may create a



Planta (2025) 261:133 Page 13 of 18 **133**

favorable biochemical environment for CA function, potentially through thiol-based regulatory mechanisms (Dreyer et al. 2020). This redox-mediated enhancement of carbon acquisition may represent a key example of how *A. rugosa* integrates environmental sensing with metabolic regulation, establishing direct molecular links between light perception, nutrient utilization, and oxidation state of key cofactors that ultimately determine enzymatic efficiency.

Our findings on the coordinated upregulation of PEPC and PEPCK under low-light conditions complement recent isotopic studies by Wieloch et al. (2022), who reported approximately 10% of glucose-6-phosphate entering the starch biosynthesis pathway was diverted into anaplerotic pathways under low CO₂ (180 ppm) conditions. While our experimental setup differs in that we examined interactive effects of light and nutrient availability rather than manipulating CO₂ concentration alone, both studies highlight the importance of anaplerotic carbon fixation as an adaptive mechanism when photosynthesis is constrained by environmental factors. This metabolic response is particularly significant for C3 plants like A. rugosa, as it represents a novel adaptation strategy that challenges conventional understanding of C3 photosynthetic metabolism. Intriguingly, this coordinated enhancement of PEPC and PEPCK resembles a partial engagement of C4-like biochemistry (Vidal et al. 2004; Bailey et al. 2007) within a C3 framework, suggesting that the evolutionary distinction between C3 and C4 metabolism may represent more of a continuum than previously recognized. The substantial increases we observed in both PEPC (110.7% higher) and PEPCK (34.3% higher) activities under low-light conditions were further modulated by nutrient availability, with the highest activities observed at the highest nutrient level (NPK4). This nutrient-dependent enhancement under low light suggests that A. rugosa can capitalize on available nitrogen resources to upregulate alternative carbon fixation pathways when Rubisco-mediated fixation is light-limited. Conversely, under high-light conditions, these enzyme activities showed different nutrient response patterns, with PEPC gradually increasing with nutrient levels while PEPCK increased most dramatically at the highest nutrient level. This complex interplay between light and nutrient availability in regulating anaplerotic pathways suggests a sophisticated metabolic integration system that optimizes carbon acquisition strategies based on the prevailing environmental constraints. While our enzyme activity measurements do not allow us to directly quantify the percentage of carbon diverted through these pathways as Wieloch et al. (2022) did with their isotopic approach, the magnitude of the changes we observed and their responsiveness to both light and nutrient gradients suggests this represents a substantial and environmentally tuned metabolic investment for C3 plants adapting to heterogeneous conditions.

A particularly revealing aspect of our study concerns the differential regulation of mitochondrial metabolism observed across light treatments. High-light plants exhibited substantially higher PDC activity than in low-light conditions, with a notable decreasing trend as nutrient levels increased. This pattern implies a strategic reallocation of carbon resources under varying nutrient availability (Plaxton and Podestá 2006; Tcherkez et al. 2012). The PDC activity in high-light conditions was elevated at lower nutrient levels, decreasing by 70.6% at the highest nutrient level, indicating a complex interplay between carbon substrate availability and nitrogen allocation (Smith and Stitt 2007). Our findings contrast with previous studies on Arabidopsis, where PDC activity increased under higher nutrient conditions (Dahal and Vanlerberghe 2018). The respiratory chain component NADH-UQ showed divergent response patterns between light regimes as nutrient levels increased. While highlight plants maintained or slightly increased NADH-UQ activity across nutrient levels, low-light plants exhibited a progressive decline in activity, culminating in a 50.5% reduction at LL-NPK4. This divergence in respiratory electron transport suggests a fundamental shift in energy metabolism strategy (Rasmusson et al. 2008), aligning with recent theoretical work by Gu (2023) demonstrating how electron transport chain optimization is critical for sustainable improvement of photosynthesis under varying environmental conditions. COX activity similarly showed marked differences between light regimes, with high-light plants maintaining significantly higher respiratory capacity. Previous studies by Florez-Sarasa et al. (2016) reported similar light-dependent regulation of COX activity in Arabidopsis, although with less pronounced differences. These patterns of respiratory enzyme regulation highlight the plant's capacity to fine-tune energy-generating pathways as per environmental limits (Schwarzländer and Finkemeier 2013; O'Leary et al. 2020).

Our investigation of cellular redox balance reveals critical insights into how A. rugosa maintains metabolic homeostasis under varying environmental conditions. The pronounced differences in NADP+/NADPH and NAD+/NADH ratios between high-light and low-light conditions highlight the fundamental role of redox status in coordinating energy metabolism. High-light adapted plants maintained significantly more oxidized states of both pyridine nucleotide pools compared to low-light plants, with 20.6% higher NADP+/NADPH and 12.8% higher NAD+/ NADH ratios. While Foyer and Noctor (2016) established that redox homeostasis serves as an integration point linking photosynthetic electron transport with carbon assimilation, our study uniquely demonstrates the concurrent regulation of both NADP+/NADPH and NAD+/NADH pools in response to combined light and nutrient gradients—a relationship not previously characterized in non-model species like A.



rugosa. Unlike previous studies that reported substantial fluctuations in both oxidized and reduced forms (Hachiya and Noguchi 2011), we observed remarkable stability in NADPH levels despite significant variations in NADP+ content across treatments. This unprecedented stability suggests A. rugosa employs specialized mechanisms to maintain reducing power for biosynthetic processes regardless of environmental perturbations. Moreover, the nutrient-dependent decrease in NAD+ content we observed at higher NPK levels differs from observations in mitochondrial complex I mutants in Arabidopsis, which typically show increased NAD pools associated with nitrogen metabolite accumulation (Rasmusson et al. 2020). This difference indicates a species-specific strategy in A. rugosa involving the potential redirection of nitrogen resources from NAD biosynthesis toward other metabolic priorities at higher nutrient levels. The strong correlations between redox ratios and key metabolic enzymes, particularly between NADP+/NADPH and COX (r = 0.74), and NAD+/NADH and CA (r = 0.76) reveal novel regulatory networks not previously documented. Our results hint at a potential redox-based mechanism regulating these key enzymes, supported for example by the work of Dreyer et al. (2020). Their study confirmed the susceptibility of CA to oxidative deactivation, likely through the formation of intramolecular disulfide bridges. While Igamberdiev and Gardeström (2003) observed redox-dependent regulation of other specific enzymes, our comprehensive correlation analysis uncovers a more extensive regulatory network integrating carbon fixation, respiratory chain components, and redox systems that appears to be distinctive to the adaptation strategy of A. rugosa.

Another key finding was the capacity of low-light plants to accumulate higher ATP levels despite reductions in respiratory activity. Compared to high-light, low-light plants had 50% lower NADH-UQ and 46% lower COX activities, suggesting a restricted flow of electrons via the mitochondrial transport chain. However, low-light plants had drastically higher ATP levels, reaching a maximum (12.88 \pm 0.84 nmol g⁻¹ FW), under high-nutrient levels (LL–NPK3) that was tenfold greater than the corresponding high-light treatment. This finding aligns with observations by Bellasio and Griffiths (2014), who reported that maize leaves re-acclimated to low light sustained substantially higher ATP levels than high-light adapted plants under low irradiance. However, it contrasts with earlier work by Prinsley et al. (1986), who found in spinach that ATP/ADP ratios decreased immediately following a decrease in irradiance and only slowly recovered to a new steady state. This paradoxical situation of greater ATP accumulation under lower respiratory flux can be rationalized by considering the dynamic balance between ATP synthesis and utilization. The elevated ATP levels in low-light plants likely reflect a decrease in consumption of this energy currency rather than an increase in production. Under light limitation, plants may actively downregulate ATP-intensive metabolic processes to conserve resources (Rott et al. 2011; Wang et al. 2021; Smith et al. 2024) leading to a net increase in steady-state ATP pool. This interpretation is supported by the strong negative correlations observed between ATP levels and markers of oxidative metabolism like NADP⁺ (r = -0.67, P < 0.001). The clustering of ATP and NADH within the low-light associated group, along with their moderate positive correlation (r =0.55, P<0.01), demonstrates the functional link between these two metabolites. NADH serves as an electron donor for mitochondrial ATP synthesis (Schertl and Braun 2014), and the accumulation of both compounds under low-light may reflect a coordinated response to maintain energy balance when photosynthetic output is reduced (Fig. 9).

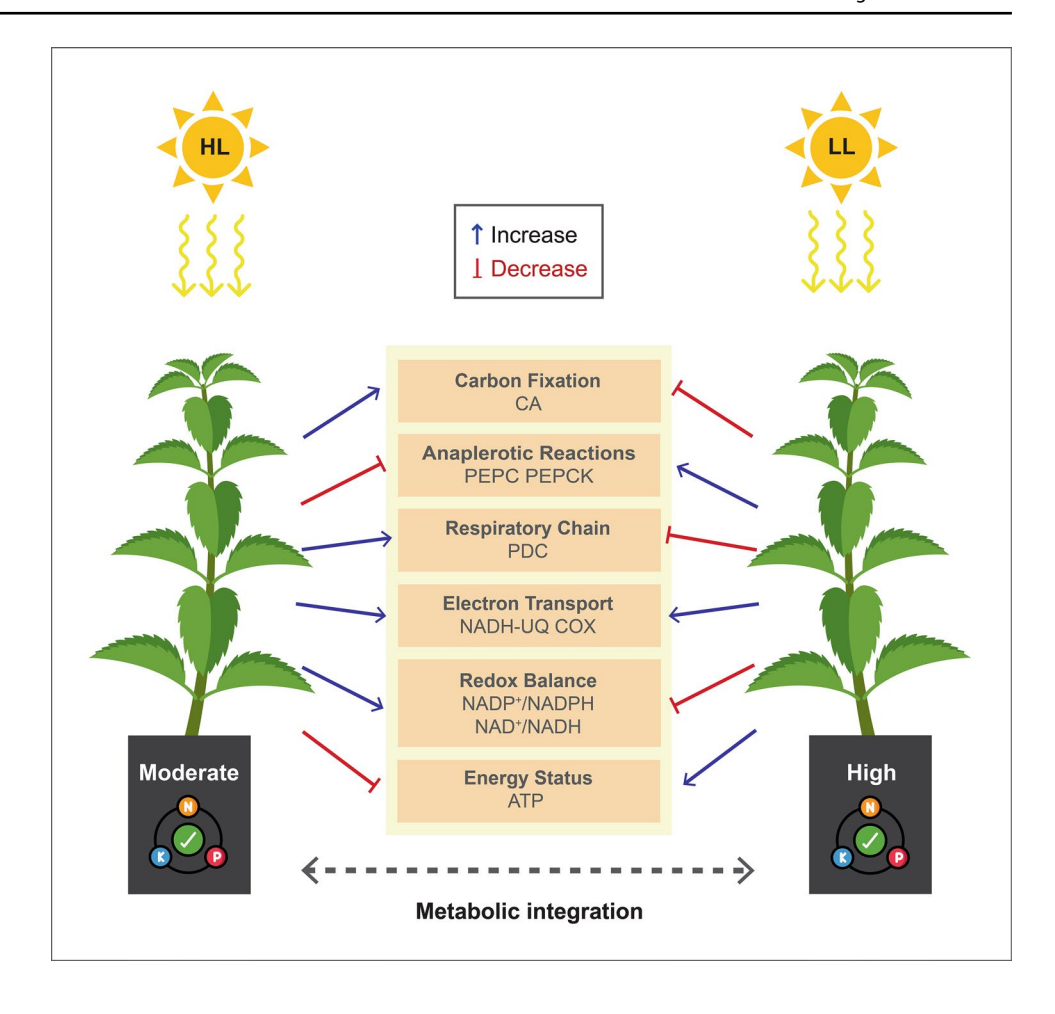
Multivariate statistical techniques, including principal component analysis (PCA) and hierarchical cluster analysis (HCA), uncovered surprising patterns of metabolic organization that transcended simple univariate relationships and demonstrated the complex interplay between light and nutrient conditions. PCA effectively partitioned light-dependent metabolic states along the first principal component (Dim1), which explained 55.5% of total variance, while nutrient-dependent responses were captured by the second principal component (Dim2), accounting for 15.7% of variance. This highlights the overriding impact of light as a key determinant of metabolic phenotype with nutrient availability playing a secondary but crucial role in modulating these responses. HCA reinforced this interpretation, with high-light associated traits like PDC and cellular redox ratios exhibiting over 70% similarity in their clustering patterns across nutrient levels. These variables formed a distinct cluster from the low-light groupings of PEPC, PEPCK, ATP, and NADH, also showing a similarity threshold exceeding 75% across nutrient levels. This robust separation underscores the divergent metabolic strategies of A. rugosa under different light regimes, while also emphasizing the modulatory influence of nutrient availability within each light environment.

While most traits that showed strong pairwise correlations were also clustered together, there were a few notable exceptions. For instance, despite significant positive correlations between PDC and the NADP+/NADPH ratio (r = 0.65, P < 0.001), these traits did not develop a unified cluster. PDC was part of the high-light associated cluster, while NADP+/NADPH grouped with other redox-related parameters in a separate cluster. Similarly, NADH exhibited a moderately strong positive correlation with ATP (r = 0.55, P < 0.01), but these traits were part of distinct low-light associated clusters. NADH clustered with ATP in one subgroup, while PEPC, and PEPCK formed another closely related branch. In this case, while PDC shows



Planta (2025) 261:133 Page 15 of 18 **133**

Fig. 9 Schematic diagram illustrating the metabolic reprogramming in A. rugosa under different light and nutrient levels. Dashed line indicates potential metabolic integration achieved via shared substrate pools, coordinated enzyme regulation and redox balance maintenance. HL high light, LL low light, CA carbonic anhydrase, PEPC phosphoenolpyruvate carboxylase, PEPCK phosphoenolpyruvate carboxykinase, PDC pyruvate dehydrogenase complex, NADH-UQ NADH-ubiquinone oxidoreductase, COX cytochrome c oxidase, NADP+ nicotinamide adenine dinucleotide phosphate, NADPH reduced nicotinamide adenine dinucleotide phosphate, NAD+ nicotinamide adenine dinucleotide, NADH reduced nicotinamide adenine dinucleotide, ATP adenosine triphosphate



positive associations with NADP+/NADPH, its overall pattern of light- and nutrient-dependent changes is more like other high-light associated traits like CA and NAD+/NADH. As a result, it clusters with these variables despite some strong pairwise correlations with traits in other groups. These nuances in clustering patterns highlight the complex, multidimensional nature of metabolic responses to environmental factors.

Several important considerations should be noted when interpreting these results. While our use of polytunnels with shade netting provided realistic light conditions, the measurements represent specific time points in the growing season and may not fully capture seasonal variations in these metabolic adaptations. Our analysis also focused on leaf tissue, and the response patterns might differ in other organs. The interaction between light and temperature in polytunnel environments could also affect some of the observed metabolic responses. A key limitation in comparison to studies like Wieloch et al. (2022) is our reliance on enzyme activity measurements rather than direct carbon flux quantification through isotopic labeling. While elevated PEPC and PEPCK activities strongly suggest increased carbon flow through anaplerotic pathways, we cannot precisely determine what

percentage of fixed carbon is diverted through these alternative routes. Additionally, although our low-light treatment produced significant metabolic reprogramming, it still provided relatively high PPFD (700–800 $\mu mol\ m^{-2}\ s^{-1})$ compared to deep shade environments, and more extreme light limitation might trigger even more pronounced responses. Future studies incorporating seasonal time-course measurements, tissue-specific analyses, and isotopic labeling techniques could help address these limitations.

This study opens several promising avenues for future research. The strong coordination between PEPC and PEPCK activities suggests the existence of shared regulatory mechanisms that warrant research at the transcriptional and post-translational levels. Identification of transcription factors and signaling components mediating this response could provide valuable insights into metabolic adaptation mechanisms. In addition, the paradoxical accumulation of ATP in low-light conditions raises intriguing questions about energy-sensing pathways and their regulation. Investigating the function of known energy sensors like SnRK1 and TOR kinases in this context could reveal novel regulatory circuits. Thus, the potential contribution of these metabolic adaptations to the secondary metabolism and medicinal



properties of *A. rugosa* remains a significant area for future exploration, particularly given this species' economic importance.

Conclusion

Our study demonstrates the intricate metabolic reprogramming employed by A. rugosa to maintain energetic and redox balance under dynamic light and nutrient environments. The clear divergence in strategies between high-light and low-light adapted plants, shown by the contrasting regulation of carbon fixation pathways and differential management of ATP and redox status, underscores the impact of light on shaping metabolic phenotypes. The unexpected synergistic upregulation of PEPC and PEPCK under low-light and the capacity to maintain higher ATP levels despite reduced respiratory activity provide compelling evidence for the existence of complex regulatory networks coordinating energy metabolism across cellular compartments. Also, the identification of optimal nutrient for achieving peak metabolic performance, like the moderate-nutrient treatment (NPK2, 80 mg kg⁻¹) under high-light levels that maximized carbonic anhydrase activity and redox balance, highlights the critical role of nutrient availability in fine-tuning these metabolic adaptations. These findings challenge conventional models of plant metabolic responses and pave the way for future studies into the molecular mechanisms of this remarkable metabolic plasticity in A. rugosa, while also offering valuable insights for optimizing the cultivation of this economically important herb.

Supplementary Information The online version contains supplementary material available at https://doi.org/10.1007/s00425-025-04710-4.

Acknowledgements This work has received funding from the Putra Graduate Initiative Grant (GP-IPS) from Universiti Putra Malaysia (GP-IPS/2018/9660900). We also acknowledge other researchers and staff for their excellent management and general skills.

Author contributions Khairul Azree Rosli: Conceptualization, Funding acquisition, Methodology, Experimentalize, Formal analysis, Data curation, Validation, Visualization, Software, Resources, Writing-original draft. Puteri Edaroyati Megat Wahab: Conceptualization, Methodology, Resources, Revision, Supervision. Azizah Misran: Resources, Revision, Supervision. Latifah Saiful Yazan: Revision, Supervision. All authors have read and revised the manuscript, provided helpful discussions, and approved its final version.

Funding Universiti Putra Malaysia, GP-IPS/2018/9660900, Puteri Edaroyati Megat Wahab

Data availability The data and materials supporting this study's findings are available from the corresponding author upon request.



Conflict of interest The authors declare that they have no known competing financial interests or personal relationships that could have appeared to influence the work reported in this paper.

References

- Alber NA, Vanlerberghe GC (2021) The flexibility of metabolic interactions between chloroplasts and mitochondria in *Nicotiana tabacum* leaf. Plant J 106:1625–1646. https://doi.org/10.1111/tpi.15259
- An JH, Yuk HJ, Kim DY et al (2018) Evaluation of phytochemicals in Agastache rugosa (Fisch. & C.A.Mey.) Kuntze at different growth stages by UPLC-QTof-MS. Ind Crops Prod 112:608–616. https://doi.org/10.1016/j.indcrop.2017.12.050
- Anand S, Pang E, Livanos G, Mantri N (2018) Characterization of physico-chemical properties and antioxidant capacities of bioactive honey produced from Australian grown *Agastache rugosa* and its correlation with colour and poly-phenol content. Molecules 23:108. https://doi.org/10.3390/molecules23010108
- Artins A, Caldana C (2022) The metabolic homeosta TOR: the balance of holding on or letting grow. Curr Opin Plant Biol 66:102196. https://doi.org/10.1016/j.pbi.2022.102196
- Bailey KJ, Gray JE, Walker RP, Leegood RC (2007) Coordinate regulation of phosphoenolpyruvate carboxylase and phosphoenolpyruvate carboxykinase by light and CO₂ during C₄ photosynthesis. Plant Physiol 144:479–486. https://doi.org/10.1104/pp.106.093013
- Balcke GU, Vahabi K, Giese J et al (2024) Coordinated metabolic adaptation of *Arabidopsis thaliana* to high light. Plant J 120:387–405. https://doi.org/10.1111/tpj.16992
- Bellasio C, Griffiths H (2014) Acclimation of C4 metabolism to low light in mature maize leaves could limit energetic losses during progressive shading in a crop canopy. J Exp Bot 65:3725–3736. https://doi.org/10.1093/jxb/eru052
- Bielecka M, Zielińska S, Pencakowski B et al (2019) Age-related variation of polyphenol content and expression of phenylpropanoid biosynthetic genes in *Agastache rugosa*. Ind Crops Prod 141:111743. https://doi.org/10.1016/j.indcrop.2019.111743
- Bowley S (1999) A hitchhiker's guide to statistics in plant biology. Any Old Subject Books, Guelph
- Bräutigam K, Dietzel L, Kleine T et al (2009) Dynamic plastid redox signals integrate gene expression and metabolism to induce distinct metabolic states in photosynthetic acclimation in *Arabidopsis*. Plant Cell 21:2715–2732. https://doi.org/10.1105/tpc.108.062018
- Burnell JN, Suzuki I, Sugiyama T (1990) Light induction and the effect of nitrogen status upon the activity of carbonic anhydrase in maize leaves. Plant Physiol 94:384–387. https://doi.org/10.1104/pp.94.1. 384
- Cardoso LL, Freire FBS, Daloso DM (2023) Plant metabolic networks under stress: a multi-species/stress condition meta-analysis. J Soil Sci Plant Nutr 23:4–21. https://doi.org/10.1007/s42729-022-01032-2
- Corti F, Festa M, Szabo I (2023) Mitochondria–chloroplast cross talk: a possible role for calcium and reactive oxygen species? Bioelectricity 5:39–46. https://doi.org/10.1089/bioe.2023.0002
- Dahal K, Vanlerberghe GC (2018) Growth at elevated CO₂ requires acclimation of the respiratory chain to support photosynthesis. Plant Physiol 178:82–100. https://doi.org/10.1104/pp.18.00712



Planta (2025) 261:133 Page 17 of 18 **133**

- Dahal K, Martyn GD, Alber NA, Vanlerberghe GC (2016) Coordinated regulation of photosynthetic and respiratory components is necessary to maintain chloroplast energy balance in varied growth conditions. J Exp Bot 68:657–671. https://doi.org/10.1093/jxb/ erw469
- DiMario RJ, Clayton H, Mukherjee A et al (2017) Plant carbonic anhydrases: structures, locations, evolution, and physiological roles. Mol Plant 10:30–46. https://doi.org/10.1016/j.molp.2016.09.001
- Dreyer A, Schackmann A, Kriznik A et al (2020) Thiol redox regulation of plant β-carbonic anhydrase. Biomolecules 10:1125. https://doi.org/10.3390/biom10081125
- Fang C, Fernie AR, Luo J (2019) Exploring the diversity of plant metabolism. Trends Plant Sci 24:83–98. https://doi.org/10.1016/j. tplants.2018.09.006
- Florez-Sarasa I, Noguchi K, Araújo WL et al (2016) Impaired cyclic electron flow around photosystem I disturbs high-light respiratory metabolism. Plant Physiol 172:2176–2189. https://doi.org/ 10.1104/pp.16.01025
- Fonseca de Lima CF, Kleine-Vehn J, De Smet I, Feraru E (2021) Getting to the root of belowground high temperature responses in plants. J Exp Bot 72:7404–7413. https://doi.org/10.1093/jxb/erab202
- Foyer CH, Noctor G (2016) Stress-triggered redox signalling: what's in pROSpect? Plant Cell Environ 39:951–964. https://doi.org/10.1111/pce.12621
- Gao F, Guo J, Shen Y (2024) Advances from chlorophyll biosynthesis to photosynthetic adaptation, evolution and signaling. Plant Stress 12:100470. https://doi.org/10.1016/j.stress.2024.100470
- Ghimire B, Riley WJ, Koven CD et al (2017) A global trait-based approach to estimate leaf nitrogen functional allocation from observations. Ecol Appl 27:1421–1434. https://doi.org/10.1002/eap.1542
- Gollan PJ, Grebe S, Roling L et al (2023) Photosynthetic and transcriptome responses to fluctuating light in *Arabidopsis* thylakoids ion transport triple mutant. Plant Direct 7:e534. https://doi.org/10.1002/pld3.534
- Gu L (2023) Optimizing the electron transport chain to sustainably improve photosynthesis. Plant Physiol 193:2398–2412. https:// doi.org/10.1093/plphys/kiad490
- Hachiya T, Noguchi K (2011) Integrative response of plant mitochondrial electron transport chain to nitrogen source. Plant Cell Rep 30:195–204. https://doi.org/10.1007/s00299-010-0955-0
- He C, Berkowitz O, Hu S et al (2023) Co-regulation of mitochondrial and chloroplast function: Molecular components and mechanisms. Plant Commun 4:100496. https://doi.org/10.1016/j.xplc.2022.100496
- Herrmann HA, Dyson BC, Vass L et al (2019) Flux sampling is a powerful tool to study metabolism under changing environmental conditions. NPJ Syst Biol Appl. https://doi.org/10.1038/s41540-019-0109-0
- Hou HD, Wu CY, Zhou J et al (2022) Holistic quality evaluation of commercial Agastache rugosa by multiple chromatographic and chemometric analysis. J Pharm Biomed Anal. https://doi.org/10. 1016/j.jpba.2021.114574
- Huang S, Lee CP, Millar AH (2015) Activity assay for plant mitochondrial enzymes. In: Whelan J, Murcha MW (eds) Plant mitochondria. Springer, New York, pp 139–149
- Igamberdiev AU, Gardeström P (2003) Regulation of NAD- and NADP-dependent isocitrate dehydrogenases by reduction levels of pyridine nucleotides in mitochondria and cytosol of pea leaves. Biochim Biophys Acta Bioenerg 1606:117–125. https://doi.org/10.1016/S0005-2728(03)00106-3
- Jänkänpää HJ, Mishra Y, Schröder WP, Jansson S (2012) Metabolic profiling reveals metabolic shifts in *Arabidopsis* plants grown under different light conditions. Plant Cell Environ 35:1824–1836. https://doi.org/10.1111/j.1365-3040.2012.02519.x

Kim SW (2020) Korean native wild herbal-based functional ingredient for skin health: Agatri[®] (*Agastache rugosa* extract). Food Sci Ind 53:382–389. https://doi.org/10.23093/FSI.2020.53.4.382

- Lawson T, Emmerson R, Battle M et al (2022) Carbon fixation. In: Ruban A, Foyer CH, Murchie EH (eds) Photosynthesis in action. Elsevier, Amsterdam, pp 31–58
- Lee Y, Lim H-W, Ryu IW et al (2020) Anti-inflammatory, barrier-protective, and antiwrinkle properties of *Agastache rugosa* Kuntze in human epidermal keratinocytes. Biomed Res Int 2020:e1759067. https://doi.org/10.1155/2020/1759067
- Li Y, Grotewold E, Dudareva N (2024) Enough is enough: feedback control of specialized metabolism. Trends Plant Sci 29:514–523. https://doi.org/10.1016/j.tplants.2023.07.012
- Lim S-L, Voon CP, Guan X et al (2020) In planta study of photosynthesis and photorespiration using NADPH and NADH/NAD+ fluorescent protein sensors. Nat Commun 11:3238. https://doi.org/ 10.1038/s41467-020-17056-0
- Mohammad F, Khan T, Afridi RM, Fatma A (1998) Effect of nitrogen on carbonic anhydrase activity, stomatal conductance, net photosynthetic rate and yield of mustard. Photosynthetica 34:595–598. https://doi.org/10.1023/A:1006882016862
- Moore KJ, Dixon PM (2015) Analysis of combined experiments revisited. Agron J 107:763–771. https://doi.org/10.2134/agronj13.0485
- Nunes-Nesi A, Fernie AR, Stitt M (2010) Metabolic and signaling aspects underpinning the regulation of plant carbon nitrogen interactions. Mol Plant 3:973–996. https://doi.org/10.1093/mp/ssq049
- O'Leary BM, Oh GGK, Lee CP, Millar AH (2020) Metabolite regulatory interactions control plant respiratory metabolism via target of rapamycin (TOR) kinase activation. Plant Cell 32:666–682. https://doi.org/10.1105/tpc.19.00157
- Plaxton WC, Podestá FE (2006) The functional organization and control of plant respiration. Crit Rev Plant Sci 25:159–198. https://doi.org/10.1080/07352680600563876
- Prinsley RT, Dietz K-J, Leegood RC (1986) Regulation of photosynthetic carbon assimilation in spinach leaves after a decrease in irradiance. Biochim Biophys Acta Bioenerg 849:254–263. https://doi.org/10.1016/0005-2728(86)90032-0
- Rasmusson AG, Geisler DA, Møller IM (2008) The multiplicity of dehydrogenases in the electron transport chain of plant mitochondria. Mitochondrion 8:47–60. https://doi.org/10.1016/j. mito.2007.10.004
- Rasmusson AG, Escobar MA, Hao M et al (2020) Mitochondrial NAD(P)H oxidation pathways and nitrate/ammonium redox balancing in plants. Mitochondrion 53:158–165. https://doi.org/10.1016/j.mito.2020.05.010
- Rott M, Martins NF, Thiele W et al (2011) ATP synthase repression in tobacco restricts photosynthetic electron transport, CO₂ assimilation, and plant growth by overacidification of the thylakoid lumen. Plant Cell 23:304–321. https://doi.org/10.1105/tpc.110.079111
- Rymen B, Sugimoto K (2012) Tuning growth to the environmental demands. Curr Opin Plant Biol 15:683–690. https://doi.org/10.1016/j.pbi.2012.07.005
- Sathee L, Suriyaprakash R, Barman D et al (2024) Nitrogen at the crossroads of light: Integration of light signalling and plant nitrogen metabolism. J Exp Bot 76:803–818. https://doi.org/10.1093/jxb/erae437
- Scheibe R (2019) Maintaining homeostasis by controlled alternatives for energy distribution in plant cells under changing conditions of supply and demand. Photosynth Res 139:81–91. https://doi.org/10.1007/s11120-018-0583-z
- Schertl P, Braun H-P (2014) Respiratory electron transfer pathways in plant mitochondria. Front Plant Sci 5:163. https://doi.org/10. 3389/fpls.2014.00163



133 Page 18 of 18 Planta (2025) 261:133

Schwarzländer M, Finkemeier I (2013) Mitochondrial energy and redox signaling in plants. Antioxid Redox Signal 18:2122–2144. https://doi.org/10.1089/ars.2012.5104

- Shen Y, Issakidis-Bourguet E, Zhou D-X (2016) Perspectives on the interactions between metabolism, redox, and epigenetics in plants. J Exp Bot 67:5291–5300. https://doi.org/10.1093/jxb/erw310
- Shi ZM, Tang JC, Cheng RM et al (2015) A review of nitrogen allocation in leaves and factors in its effects. Acta Ecol Sinica 35:5909-5919
- Smith AM, Stitt M (2007) Coordination of carbon supply and plant growth. Plant Cell Environ 30:1126–1149. https://doi.org/10.1111/j.1365-3040.2007.01708.x
- Smith K, Strand DD, Walker BJ (2024) Evaluating the contribution of plant metabolic pathways in the light to the ATP:NADPH demand using a meta-analysis of isotopically non-stationary metabolic flux analyses. Photosynth Res 161:177–189. https://doi.org/10.1007/ s11120-024-01106-5
- Stitt M, Krapp A (1999) The interaction between elevated carbon dioxide and nitrogen nutrition: the physiological and molecular background. Plant Cell Environ 22:583–621. https://doi.org/10.1046/j.1365-3040.1999.00386.x
- Suzuki N, Koussevitzky S, Mittler R, Miller G (2012) ROS and redox signalling in the response of plants to abiotic stress. Plant Cell Environ 35:259–270. https://doi.org/10.1111/j.1365-3040.2011. 02336.x
- Tcherkez G, Boex-Fontvieille E, Mahé A, Hodges M (2012) Respiratory carbon fluxes in leaves. Curr Opin Plant Biol 15:308–314. https://doi.org/10.1016/j.pbi.2011.12.003
- Thiellement H (2010) Plant proteomics: Methods and protocols. Humana Press, Heidelberg
- Tiwari A, Kumar P, Chawhaan PH et al (2006) Carbonic anhydrase in *Tectona grandis*: Kinetics, stability, isozyme analysis and relationship with photosynthesis. Tree Physiol 26:1067–1073. https://doi.org/10.1093/treephys/26.8.1067
- Trugman AT, Anderegg LDL (2025) Source vs sink limitations on tree growth: from physiological mechanisms to evolutionary constraints and terrestrial carbon cycle implications. New Phytol 245:966–981. https://doi.org/10.1111/nph.20294
- VanWallendael A, Soltani A, Emery NC et al (2019) A molecular view of plant local adaptation: incorporating stress-response networks. Annu Rev Plant Biol 70:559–583. https://doi.org/10.1146/annur ev-arplant-050718-100114
- Vargas M, Glaz B, Alvarado G et al (2015) Analysis and interpretation of interactions in agricultural research. Agron J 107:748–762. https://doi.org/10.2134/agronj13.0405
- Vidal J, Bakrim N, Hodges M (2004) The regulation of plant phosphoenolpyruvate carboxylase by reversible phosphorylation. In: Foyer CH, Noctor G (eds) Photosynthetic nitrogen assimilation and associated carbon and respiratory metabolism. Kluwer Academic Publishers, Dordrecht, pp 135–150

- Wang Y, Selinski J, Mao C et al (2020) Linking mitochondrial and chloroplast retrograde signalling in plants. Philos Trans R Soc B Biol Sci 375:20190410. https://doi.org/10.1098/rstb.2019.0410
- Wang C, Xiang Y, Qian D (2021) Current progress in plant V-ATPase: From biochemical properties to physiological functions. J Plant Physiol. https://doi.org/10.1016/j.jplph.2021.153525
- Weng J-K, Lynch JH, Matos JO, Dudareva N (2021) Adaptive mechanisms of plant specialized metabolism connecting chemistry to function. Nat Chem Biol 17:1037–1045. https://doi.org/10.1038/s41589-021-00822-6
- Wieloch T, Augusti A, Schleucher J (2022) Anaplerotic flux into the Calvin-Benson cycle: hydrogen isotope evidence for in vivo occurrence in C3 metabolism. New Phytol 234:405–411. https://doi.org/10.1111/nph.17957
- Wilbur KM, Anderson NG (1948) Electrometric and colorimetric determination of carbonic anhydrase. J Biol Chem 176:147–154. https://doi.org/10.1016/S0021-9258(18)51011-5
- Yamani H, Mantri N, Morrison PD, Pang E (2014) Analysis of the volatile organic compounds from leaves, flower spikes, and nectar of Australian grown *Agastache rugosa*. BMC Complement Altern Med 14:495. https://doi.org/10.1186/1472-6882-14-495
- Zandalinas SI, Balfagón D, Gómez-Cadenas A, Mittler R (2022) Plant responses to climate change: metabolic changes under combined abiotic stresses. J Exp Bot 73:3339–3354. https://doi.org/10.1093/jxb/erac073
- Zielińska S, Kolniak-Ostek J, Dziadas M et al (2016) Characterization of polyphenols in *Agastache rugosa* leaves and inflorescences by UPLC–qTOF–MS following FCPC separation. J Liq Chromatogr Relat Technol 39:209–219. https://doi.org/10.1080/10826076. 2016.1147461

Publisher's Note Springer Nature remains neutral with regard to jurisdictional claims in published maps and institutional affiliations.

Springer Nature or its licensor (e.g. a society or other partner) holds exclusive rights to this article under a publishing agreement with the author(s) or other rightsholder(s); author self-archiving of the accepted manuscript version of this article is solely governed by the terms of such publishing agreement and applicable law.

